Applied Physics Letters

Are monodisperse phospholipid-coated microbubbles "mono-acoustic?"

Sander Spiekhout ⬤ ; Benjamin van Elburg ⬤ ; Jason Voorneveld ⬤ ; Nico de Jong; Michel Versluis ⬤ ;
Johannes G. Bosch ⬤ ; Tim Segers ✉ ⬤

Check for updates

View
Online

Export
Citation

Applied Physics Letters

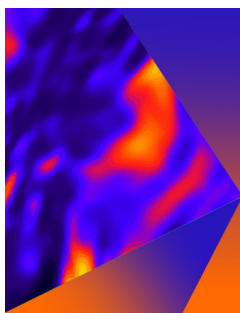Special Topic: Mid and Long Wavelength
Infrared Photonics, Materials, and Devices

Submit Today

AIP Publishing

Are monodisperse phospholipid-coated microbubbles "mono-acoustic?"

View Online   Export Citation   CrossMark

Sander Spiekhout,[1] (iD) Benjamin van Elburg,[2] (iD) Jason Voorneveld,[1] (iD) Nico de Jong,[1,3] Michel Versluis,[2] (iD)
Johannes G. Bosch,[1] (iD) and Tim Segers[4,a)] (iD)

AFFILIATIONS

[1]Biomedical Engineering, Erasmus Medical Center, Rotterdam, The Netherlands
[2]Physics of Fluids Group, TechMed Center, University of Twente, Enschede, The Netherlands
[3]Laboratory of Medical Imaging, Delft University of Technology, Delft, The Netherlands
[4]BIOS/Lab on a Chip Group, Max Planck Center Twente for Complex Fluid Dynamics, University of Twente, Enschede,
 The Netherlands

[a)]Author to whom correspondence should be addressed: t.j.segers@utwente.nl

ABSTRACT

Phospholipid-coated microbubbles with a uniform acoustic response are a promising avenue for functional ultrasound sensing. A uniform acoustic response requires both a monodisperse size distribution and uniform viscoelastic shell properties. Monodisperse microbubbles can be produced in a microfluidic flow focusing device. Here, we investigate whether such monodisperse microbubbles have uniform viscoelastic shell properties and thereby a uniform "mono-acoustic" response. To this end, we visualized phase separation of the DSPC and DPPE-PEG5000 lipid shell components and measured the resonance curves of nearly 2000 single and freely floating microbubbles using a high-frequency acoustic scattering technique. The results demonstrate inhomogeneous phase-separated shell microdomains across the monodisperse bubble population, which may explain the measured inhomogeneous viscoelastic shell properties. The shell viscosity varied over an order of magnitude and the resonance frequency by a factor of two indicating both a variation in shell elasticity and in initial surface tension despite the relatively narrow size distribution.

Lipid-coated microbubbles are used as ultrasound contrast agents (UCAs) in contrast-enhanced ultrasound imaging.[1] The contrast enhancement results from their ultrasound-driven volumetric oscillations, which produce a powerful echo. The volumetric oscillation dynamics is governed by resonance, with a resonance frequency that is inversely proportional to the microbubble size.[2] Additionally, the resonance frequency is strongly affected by the viscoelastic properties of the microbubble shell that can be modeled as an isotropic, infinitely thin membrane with a surface viscosity, resulting in an increased damping, and with a surface elasticity, which increases the resonance frequency.[3–5] At resonance, the amplitude of oscillation and the resulting echo are at maximum. Also, at resonance (or integer multiples or fractions thereof), the echo can contain strong harmonics of the driving frequency.[6] Harmonics are generated already at low acoustic driving pressures (<40 kPa) owing in particular to the nonlinear elasticity of the shell, which can vanish both upon compression and expansion of the bubble surface.[7–9]

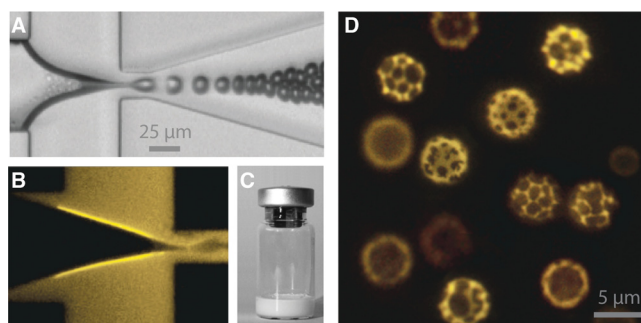
FIG. 1. (a) The flow-focusing device employed for monodisperse microbubble formation. (b) Fluorescence image showing that the lipid coating self-assembles at the gas–liquid interface before bubble pinch off. (c) The formed bubbles are collected in a glass vial. (d) The addition of a lipophilic dye shows that the monodisperse bubbles have inhomogeneous phase separated shell microstructures.

Today, the harmonic content of the bubble echo is used to discriminate nonlinear bubble echoes from linear tissue echoes and to thereby visualize the perfusion of organs.[10] However, the rich spectral content of the echo has a larger potential, owing to its sensitivity to the ambient pressure[6] and to whether the bubble is bound to an interface or not, e.g., via targeting ligands incorporated in the bubble shell.[11–13] As such, bubbles have potential blood pressure[14] and molecular sensing capabilities[15] that reach beyond their current use as a blood pool agent. However, clinically approved UCAs are non-uniform in size[1] (1–10 μm in diameter) and in shell properties[16] resulting in an ill-defined acoustic response[17,18] that prevents accurate sensing with microbubbles and ultrasound.[1,19]

The first challenge in achieving a uniform acoustic response involves the production of a suspension of microbubbles that are uniform in size. Such a monodisperse microbubble suspension can be formed in a microfluidic flow focusing device. In this device, a gas thread is focused between a co-flow through a constriction where it destabilizes and pinches off to release monodisperse bubbles [Fig. 1(a)].[20–22] However, it has been shown that when these bubbles are coated with lipids, they exhibit an inherent instability after pinch off and are prone to both coalescence and Ostwald ripening when formed at clinically relevant production rates [$\mathcal{O}(10^6$ bubbles/s)].[23–27] Only recently, these stability and production rate issues have been overcome by (i) producing bubbles at an elevated temperature,[28] (ii) filling them with a gas mixture of a low and high aqueous solubility gas,[29] and (iii) through the use of a specific lipid formulation with a long-chain PEGylated lipid (PEG5000).[30] Now that control over the bubble size distribution is established, the most pressing yet unaddressed question that we aim to answer in this Letter is: Are monodisperse phospholipid-coated microbubbles mono-acoustic? In other words, do they have uniform shell properties and therefore a uniform acoustic response?

The monodisperse microbubble suspension characterized in the present work was formed in the flow focusing device shown in Fig. 1(a)[9] at a temperature of 60 °C to minimize on-chip bubble coalescence.[28] The co-flow comprised our standard lipid mixture with the primary phospholipid DSPC and the PEGylated phospholipid DPPE-PEG5000 (Corden Pharma, Liestal, Switzerland) mixed at a 9 to 1 molar ratio at a total concentration of 12.5 mg per mL of air-saturated saline. The rationale for this composition is provided by Segers et al.[29] The lipid dispersion (prepared as before[30]) adsorbs to the gas liquid interface already before bubble pinch off [Fig. 1(b)]. However, the lipids self-assemble at a relatively low packing density resulting in partial bubble dissolution, which mechanically compresses the lipid shell until a stable bubble is formed.[26] To mitigate foam formation via Ostwald ripening during bubble stabilization in the collection vial [Fig. 1(c)], the bubbles were initially filled with a gas mixture of 12 vol. % of C_4F_{10} in CO_2. Once stabilized, the gas core comprised nearly pure C_4F_{10}.[29] The bubble concentration in the collection vial was measured using a Coulter Counter (Multisizer 4e, Beckman) to be 300 million bubbles per mL, where one mL was produced in 6 min.

We start our investigation on the uniformity of the shell properties by adding 0.01 mol. % of lipophilic fluorescent dye (Rhodamine DHPE, Thermo Fischer Scientific) to the lipid formulation to visualize potential phase separation of condensed and expanded domains in the shell, which has been observed to occur for similar lipid mixtures.[31,32] Indeed, Fig. 1(d) demonstrates that phase separation also occurs in the
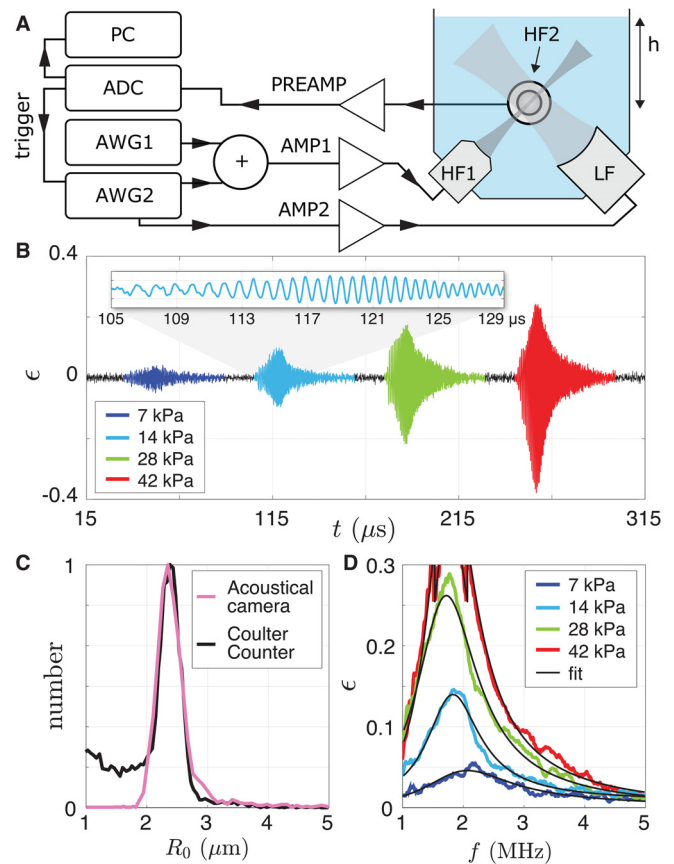

FIG. 2. (a) Schematic of the acoustical camera (AC). A high-frequency (HF) 25-MHz probing wave is transmitted (HF1) and its scattering by a bubble is recorded by HF2 (axis into the paper) to obtain the (b) radial strain ϵ of the microbubble in response to a low-frequency (LF) chirp. (c) Equilibrium bubble radius R_0 from phase demodulation in the AC[33] (pink curve) is in excellent agreement with that measured using a Coulter Counter (black curve). The shoulder at $R_0 < 2\,\mu$m (black curve) is due to lipid aggregates instead of bubbles. (d) Envelopes of the radial strain shown in (b) (same color coding) plotted together with a fit of a linearized bubble dynamics model.

shell of microfluidically formed monodisperse bubbles. The dark domains are generally understood to represent the condensed phase, which is potentially enriched in primary lipid, while the bright inter-domain regions are believed to be in the less densely packed liquid expanded phase, potentially enriched in PEGylated lipid (and fluorescent dye).[31,32] Remarkably, the phase separated microstructures observed in Fig. 1(d) are heterogeneous across the bubble population even though the bubbles were formed one-by-one under exactly the same microfluidic conditions.

To characterize the viscoelastic shell properties of the monodisperse bubbles, we measured resonance curves of individual freely floating bubbles using a high-frequency (HF) off resonance geometrical acoustic scattering technique named the "acoustical camera" (AC).[33,34] The AC setup as implemented in the present work consists of a water tank [Fig. 2(a), h = 26 cm, total volume = 1.8 L] with three confocally aligned and perpendicularly mounted transducers: HF1, HF2, and LF. The high-frequency transducers (HF1 and HF2) were identical

(V324-SU, Olympus) with a 25 MHz center frequency, 67% bandwidth, 6.35 mm aperture, 25.4 mm focal distance, and a FWHM lateral focal width of 0.2 mm. The low-frequency (LF) transducer (PA275, Precision Acoustics) has a 5-MHz center frequency, 160% bandwidth, 25.4 mm aperture, and a FWHM lateral focal width of 1.4 mm at 2 MHz. The output acoustic pressure sensitivities of HF1 and LF were calibrated using a needle hydrophone (0.2 mm, Precision Acoustics, uncertainty of 13%–17%). The tank was filled with the microbubble suspension diluted in saline with a temperature of 20 °C to a concentration of 300 bubbles/mL. The suspension was continuously stirred such that by chance, a single microbubble passed through the confocal transducer region where its presence was detected by transducer HF2 from the geometrical scattering of a 10-cycle, 25-MHz detection pulse with a peak negative pressure amplitude (PNP) of 500 kPa transmitted 250 times/s by transducer HF1. The frequency of the 25-MHz detection pulse is 10 times higher than the resonance frequencies of the microbubbles under investigation, and it therefore does not induce volumetric bubble oscillations. When the amplitude of the HF scattering signal exceeded the electrical noise of the system by 28 dB, the full bubble characterization sequence was transmitted. The characterization sequence consisted of an 8375-cycle (335 μs) HF probing burst transmitted by HF1 with a frequency of 25 MHz and a PNP of 500 kPa. During this HF probing burst, a sequence of four successive 50-μs low frequency (LF) linear chirps (1–5 MHz, chirp rate 80 kHz/μs) was transmitted by transducer LF to drive the bubble into volumetric oscillations. The four LF chirps were each Tukey tapered over their first and last 3 μs, spaced by 20 μs, and their PNP was kept constant in the transmit frequency range of 1.24–4.76 MHz though deconvolution of the chirps with the hydrophone-measured impulse response of the transducer[34] at acoustic pressures of 7, 14, 28, and 42 kPa. The relative radial strain of the microbubble in response to the LF driving $[\epsilon = (R(t) - R_0)/R_0]$ was obtained by amplitude demodulation of the scattered HF probing burst received by HF2, where the HF scattered amplitude is directly proportional to the microbubble size (geometrical scattering regime).[34]

A total of 1932 bubble signals was obtained during five measurement sets. Each set had a duration of 20 mins and was performed on a freshly diluted bubble suspension. Out of the 1932 detected bubbles, 1620 bubble signals were selected for further processing based on the amplitude difference of 37.5 μs of HF scattering before and after the first and final LF chirp, respectively. The amplitude difference was allowed to be <50% ensuring that the bubble did not move out of the focal region of the HF transducers, which is small as compared to the focal region of the LF transducer. The selected HF scattering signals were then bandpass filtered around the 25-MHz probing frequency (10–40 MHz). Subsequently, the modulus of the analytic signal was calculated to provide the envelope of the probe signal. From the envelope, the average HF scattering level P_{HF} was determined and the radial strain ϵ was obtained as follows: $\epsilon = (P_{LF} - P_{HF})/P_{HF}$, where P_{LF} is the envelope of the probe signal during LF insonation.[34] A typical example of ϵ is shown in Fig. 2(b), where the strain of a single bubble is plotted in response to the chirp excitation pulses at PNPs of 7 kPa (dark blue curve), 14 kPa (light blue curve), 28 kPa (green curve), and 42 kPa (red curve). The resting radius R_0 of the bubble was 2.3 μm, and it was obtained through phase demodulation of the HF scattering signal.[33] The bubble size distribution of all processed bubbles as found by the AC is plotted in Fig. 2(c) (pink curve), and it is in excellent
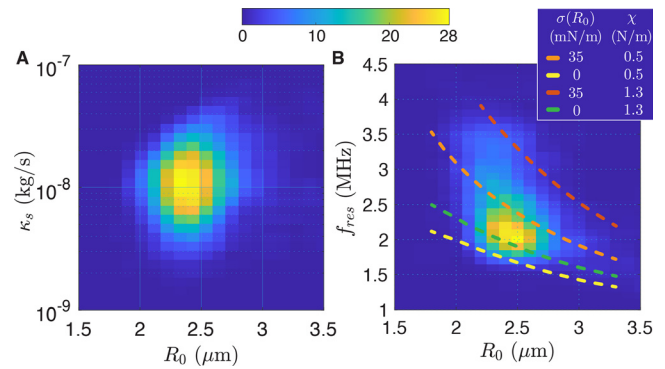

FIG. 3. (a) Shell viscosity κ_s distribution as a function of bubble radius R_0 measured for almost 2000 bubbles. The color in the colorbar indicates the number of bubbles. (B) Resonance frequency distribution as a function of R_0 and simulated $f_{res}(R_0)$ relations for different initial surface tensions and shell elasticities.

agreement with that measured using a Coulter Counter (black curve). The polydispersity index is 7% (PDI: standard deviation of the size distribution divided by the mean radius).

The envelopes of the strain responses, or resonance curves, are plotted in Fig. 2(d). In addition to the expected increase in strain with an increase in PNP, also the resonance frequency of the bubble decreases as expected, due to the averaging out of the shell elasticity over regions with and without elasticity.[5] The resonance curves were used to obtain the shell properties of individual bubbles. To this end, we employ a nonlinear Rayleigh–Plesset-type bubble dynamics equation modified with pressure terms accounting for shell viscoelasticity,[3]

$$\rho\left(\ddot{R}R + \frac{3}{2}\dot{R}^2\right) = \left(P_0 + \frac{2\sigma(R_0)}{R_0}\right)\left(\frac{R_0}{R}\right)^{3\kappa}$$
$$- P_0 - P_A(t) - \frac{2\sigma(R)}{R} - \frac{4\mu\dot{R}}{R} - \frac{4\kappa_s\dot{R}}{R^2}, \quad (1)$$

where ρ is the liquid density, μ the liquid viscosity, κ the polytropic exponent of the gas inside the bubble, P_0 the ambient pressure, and $P_A(t)$ the LF acoustic driving pressure pulse. R is the time-dependent radius of the bubble, and the overdots denote its time derivatives. κ_s is the viscosity of the shell. The surface tension is described by $\sigma(R)$, with $\sigma(R_0)$ the surface tension of the bubble interface at rest (initial surface tension). Equation (1) can be linearized to obtain the relative radial strain ϵ at small amplitudes of oscillation,[35]

$$\epsilon(\omega) = \frac{A}{\sqrt{(1 - (\omega/\omega_0)^2)^2 + (\delta_{tot}\omega/\omega_0)^2}}; \quad A = \frac{P_A}{\rho\omega_0^2 R_0^2}, \quad (2)$$

where $\omega = 2\pi f$ is the angular ultrasound frequency and ω_0 the angular eigenfrequency of the bubble,

$$\omega_0 = \frac{1}{R_0}\sqrt{\frac{1}{\rho}\left(3\kappa P_0 + (3\kappa - 1)\frac{2\sigma(R_0)}{R_0} + \frac{4\chi}{R_0}\right)}, \quad (3)$$

with χ the shell elasticity. The total damping δ_{tot} is the sum of the individual damping contributions due to acoustic re-radiation δ_{rad}, viscous dissipation in the liquid δ_{vis}, and viscous dissipation in the shell,

$$\delta_{rad} = \frac{\omega_0 R_0}{c}, \quad \delta_{vis} = \frac{4\mu}{\rho \omega_0 R_0^2}, \quad \delta_{shell} = \frac{4\kappa_s}{\rho \omega_0 R_0^3}, \qquad (4)$$

where c is the speed of sound in the liquid. For the 2.4-μm radius bubbles considered in this work [Fig. 2(c)], thermal damping δ_{th} due to heat diffusion[36,37] is nearly identical to δ_{vis} of a bubble in water.[5,37] As such, we follow a common approach of doubling the viscosity of the water to account for thermal damping.[8,38] The total damping reduces the resonance frequency of the bubble f_{res} typically by a few percent with respect to f_0, as follows:

$$f_{res} = f_0 \sqrt{1 - \delta_{tot}^2/2}. \qquad (5)$$

The linearized model [Eqs. (2)–(4)] is used first. It is fitted (RMS error minimization in MATLAB) to each resonance curve obtained at the lowest PNP of 7 kPa to obtain κ_s and f_{res} of individual bubbles. In the fitting procedure, A in Eq. (2) was a free parameter to account for uncertainties in the acoustic driving pressure P_A as well for nonlinear bubble dynamics.[39] Typical model fits are shown in Fig. 2(d) (solid black lines). The obtained κ_s and f_{res} for all bubbles were then plotted as a function of time (see supplementary material) showing that both f_{res} and κ_s did not drift over the 20 min duration of the measurement highlighting the stability of the ensemble of microbubbles. The distributions of κ_s and f_{res} as a function of R_0 for all characterized bubbles are plotted in Figs. 3(a) and 3(b), respectively. The figures demonstrate that for the narrow-sized bubble suspension with a mean radius of 2.4 μm that was characterized in the present work, remarkably, κ_s varied over as much as one order of magnitude, from 2×10^{-9} up to 2×10^{-8} kg/s, and f_{res} by a factor of 2, from 1.7 up to 3.5 MHz. Thus, the microfluidically formed monodisperse bubbles characterized in this work are not mono-acoustic due to a variation in the bubble shell viscoelastic properties.

The range of κ_s values corresponds to a decreased resonance frequency by 1%–9% [Eq. (5)]. Thus, the measured variation in f_{res} by a factor of two must have mainly resulted from variations in χ and/or $\sigma(R_0)$ [Eq. (3)]. To disentangle the effects of χ and $\sigma(R_0)$, we solve the non-linear bubble dynamics equation [Eq. (1)] to obtain f_{res} using the same chirp driving pulse as in the measurements. We first use a constant value for χ of 0.5 N/m, while $\sigma(R_0)$ was either set to 35 mN/m or zero, see the orange and yellow dashed curves in Fig. 3(b), respectively. A χ of 0.5 N/m was selected as it is the shell elasticity obtained for a suspension of bubbles with a very similar shell composition.[9] Note that the higher range of measured f_{res} is not captured by a χ of 0.5 N/m. As such, second, we plot numerically obtained curves for a χ of 1.3 N/m, while again, $\sigma(R_0)$ is either set to 35 mN/m or zero, see red and green dashed curves, respectively. A comparison between the modeled curves and the measured spread in f_{res} demonstrates that the spread in f_{res} cannot be explained by either a variation in χ or $\sigma(R_0)$ alone. Thus, across the bubble population, the microfluidically formed bubbles in the present work had not only a range of shell viscosities, but also a range of shell elasticities, as well as a range of initial surface tensions.

Finally, we turn our attention to bubble dynamics at the higher acoustic driving pressures employed here. Figure 4(a) shows the distribution of f_{res} of the entire bubble population obtained as before for PNPs of 7, 14, 28, and 42 kPa. Note that the figure shows that the distribution of f_{res} becomes narrower when the PNP increases. This is expected because an increase in strain reduces the role of the viscoelastic shell on the bubble dynamics.[5] Also note that, as before for a single
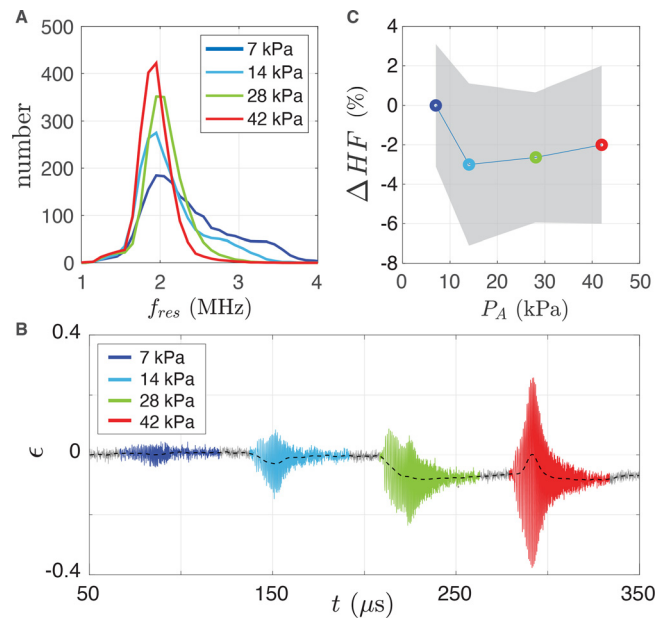
FIG. 4. (a) Resonance frequency distributions of all bubbles in the population. (b) The HF scattering response of an individual bubble often decreased during acoustic driving at PNPs >7 kPa. (c) Mean (dots) and standard deviation (gray shaded area) of the change in HF scattering signal over the LF driving bursts as a function of the PNP.

bubble [Fig. 2(d)], f_{res} shifts toward a lower frequency when the PNP increased. However, at a PNP of 28 kPa, the distribution of f_{res} peaks, unexpectedly, at a higher frequency than that at both the lower PNP of 14 kPa and the higher PNP of 42 kPa. This observation shows that the microbubbles must have changed in size and/or shell properties during the measurement. Indeed, a change in HF scattering signal was often observed during acoustic driving. A typical example is shown in Fig. 4(b), showing a decrease in HF scattering during the 28 kPa driving pulse. In Fig. 4, we plot the change in HF scattering signal ΔHF over the LF driving pulses as a function of their PNPs. The figure shows that generally no change is observed for the 7 kPa pulse, whereas at all higher acoustic driving pressures, the HF scattering signal on average decreases during the chirp driving pulse. As such, it can be concluded that acoustic driving alters the size of the bubble by 2% on average, through acoustically driven dissolution. Such a small size change results in a resonance frequency increase by only 20 kHz ($\sim$1%)[2] for a 2.4-μm radius bubble driven at the higher employed PNPs, where the effective shell elasticity approaches zero. However, the small size change may dramatically change the nonlinear acoustic response and in particular the generation of subharmonics, e.g., via a decreased $\sigma(R_0)$[8] and/or an increased χ through lipid shedding.[26] Thus, future work is required to increase bubble stability under ultrasound insonation.

To summarize, we have shown that DSPC and DPPE-PEG5000 (9:1 molar ratio) coated monodisperse microbubbles formed by microfluidic flow focusing using the protocols presented here have (i) nonuniform phase separated shell microstructures, (ii) nonuniform viscoelastic shell properties, and (iii) nonuniform acoustically driven

dissolution behavior. These intriguing conclusions raise many questions as to the nucleation and growth of shell domains,[40] whether the spread in the obtained shell properties originates from the inhomogeneous shell microstructures, and how bubble stability can be enhanced. The characterization setup presented here is a convenient method in search for answers to the open questions and to thereby come to monodisperse bubble suspensions with a high degree of monoacousticity.

See the supplementary material for details of the plots of the obtained shell viscosity and resonance frequency as a function of time.

AUTHOR DECLARATIONS
Conflict of Interest

The authors have no conflicts to disclose.

Author Contributions

Sander Spiekhout: Data curation (equal); Formal analysis (equal); Investigation (equal); Methodology (equal); Software (equal); Validation (equal); Visualization (equal); Writing – original draft (equal); Writing – review & editing (equal). **Benjamin Van Elburg:** Data curation (equal); Formal analysis (equal); Investigation (equal); Methodology (equal); Resources (equal); Software (equal); Validation (equal); Visualization (equal); Writing – original draft (equal); Writing – review & editing (equal). **Jason Voorneveld:** Formal analysis (equal); Investigation (equal); Methodology (equal); Project administration (equal); Resources (equal); Software (equal); Supervision (equal); Validation (equal); Visualization (equal); Writing – original draft (equal); Writing – review & editing (equal). **Nico de Jong:** Conceptualization (equal); Data curation (equal); Formal analysis (equal); Funding acquisition (equal); Investigation (equal); Methodology (equal); Project administration (equal); Resources (equal); Software (equal); Supervision (equal); Validation (equal); Visualization (equal); Writing – original draft (equal); Writing – review & editing (equal). **Michel Versluis:** Conceptualization (equal); Data curation (equal); Formal analysis (equal); Funding acquisition (equal); Investigation (equal); Methodology (equal); Project administration (equal); Resources (equal); Software (equal); Supervision (equal); Validation (equal); Visualization (equal); Writing – original draft (equal); Writing – review & editing (equal). **Johannes G. Bosch:** Conceptualization (equal); Data curation (equal); Formal analysis (equal); Funding acquisition (equal); Investigation (equal); Methodology (equal); Project administration (equal); Resources (equal); Software (equal); Supervision (equal); Validation (equal); Visualization (equal); Writing – original draft (equal); Writing – review & editing (equal). **Tim Segers:** Conceptualization (lead); Data curation (lead); Formal analysis (lead); Funding acquisition (lead); Investigation (lead); Methodology (lead); Project administration (lead); Resources (lead); Software (lead); Supervision (lead); Validation (lead); Visualization (lead); Writing – original draft (lead); Writing – review & editing (lead).

DATA AVAILABILITY

The data that support the findings of this study are available from the corresponding author upon reasonable request.

REFERENCES

[1] P. Frinking, T. Segers, Y. Luan, and F. Tranquart, Ultrasound Med. Biol. **46**, 892 (2020).
[2] M. Minnaert, Philos. Mag. **16**, 235 (1933).
[3] P. Marmottant, S. Van Der Meer, M. Emmer, M. Versluis, N. De Jong, S. Hilgenfeldt, and D. Lohse, J. Acoust. Soc. Am. **118**, 3499 (2005).
[4] K. Sarkar, W. T. Shi, D. Chatterjee, and F. Forsberg, J. Acoust. Soc. Am. **118**, 539 (2005).
[5] M. Versluis, E. Stride, G. Lajoinie, B. Dollet, and T. Segers, Ultrasound Med. Biol. **46**, 2117 (2020).
[6] P. J. A. Frinking, E. Gaud, J. Brochot, and M. Arditi, IEEE Trans. Ultrason., Ferroelectr., Freq. Control **57**, 1762 (2010).
[7] N. de Jong, M. Emmer, C. T. Chin, A. Bouakaz, F. Mastik, D. Lohse, and M. Versluis, Ultrasound Med. Biol. **33**, 653–656 (2007).
[8] J. Sijl, B. Dollet, M. Overvelde, V. Garbin, T. Rozendal, N. de Jong, D. Lohse, and M. Versluis, J. Acoust. Soc. Am. **128**, 3239 (2010).
[9] T. Segers, E. Gaud, M. Versluis, and P. Frinking, Soft Matter **14**, 9550 (2018).
[10] M. A. Averkiou, M. F. Bruce, J. E. Powers, P. S. Sheeran, and P. N. Burns, Ultrasound Med. Biol. **46**, 498 (2020).
[11] M. Overvelde, V. Garbin, B. Dollet, N. de Jong, D. Lohse, and M. Versluis, Ultrasound Med. Biol. **37**, 1500 (2011).
[12] B. Dollet, P. Marmottant, and V. Garbin, Ann. Rev. Fluid Mech. **51**, 331 (2019).
[13] J. S. Lum, V. Daeichin, D. F. Kienle, D. K. Schwartz, T. W. Murray, and M. A. Borden, Appl. Phys. Lett. **116**, 123703 (2020).
[14] I. Gupta, J. R. Eisenbrey, P. Machado, M. Stanczak, C. E. Wessner, C. M. Shaw, S. Gummadi, J. M. Fenkel, A. Tan, C. Miller et al., Radiology **298**, 104 (2021).
[15] A. L. Klibanov, Invest. Radiol. **41**, 354 (2006).
[16] T. Segers and M. Versluis, Lab. Chip **14**, 1705 (2014).
[17] T. Segers, P. Kruizinga, M. Kok, G. Lajoinie, N. de Jong, and M. Versluis, Ultrasound Med. Biol. **44**, 1482 (2018).
[18] A. Helbert, E. Gaud, T. Segers, C. Botteron, P. Frinking, and V. Jeannot, Ultrasound Med. Biol. **46**, 3339 (2020).
[19] N. Deshpande, A. Needles, and J. K. Willmann, Clin. Radiol. **65**, 567 (2010).
[20] A. M. Gañán-Calvo and J. M. Gordillo, Phys. Rev. Lett. **87**, 274501 (2001).
[21] S. L. Anna, N. Bontoux, and H. A. Stone, Appl. Phys. Lett. **82**, 364 (2003).
[22] P. Garstecki, H. A. Stone, and G. M. Whitesides, Phys. Rev. Lett. **94**, 164501 (2005).
[23] E. Talu, M. Lozano, R. Powell, P. Dayton, and M. Longo, Langmuir **22**, 9487 (2006).
[24] K. Hettiarachchi, E. Talu, M. L. Longo, P. A. Dayton, and A. P. Lee, Lab Chip **7**, 463 (2007).
[25] M. Parhizkar, M. Edirisinghe, and E. Stride, Microfluid. Nanofluid. **14**, 797 (2013).
[26] T. Segers, L. de Rond, N. de Jong, M. Borden, and M. Versluis, Langmuir **32**, 3937 (2016).
[27] R. Shih and A. P. Lee, Langmuir **32**, 1939 (2016).
[28] T. Segers, A. Lassus, P. Bussat, E. Gaud, and P. Frinking, Lab Chip **19**, 158 (2019).
[29] T. Segers, E. Gaud, G. Casqueiro, A. Lassus, M. Versluis, and P. Frinking, Appl. Phys. Lett. **116**, 173701 (2020).
[30] T. Segers, D. Lohse, M. Versluis, and P. Frinking, Langmuir **33**, 10329 (2017).
[31] M. A. Borden, G. V. Martinez, J. Ricker, N. Tsvetkova, M. Longo, R. J. Gillies, P. A. Dayton, and K. W. Ferrara, Langmuir **22**, 4291 (2006).
[32] S. A. Langeveld, C. Schwieger, I. Beekers, J. Blaffert, T. van Rooij, A. Blume, and K. Kooiman, Langmuir **36**, 3221 (2020).
[33] S. Spiekhout, J. Voorneveld, B. Van Elburg, G. Renaud, T. Segers, G. P. Lajoinie, M. Versluis, M. D. Verweij, N. De Jong, and J. G. Bosch, J. Acoust. Soc. Am. **151**, 3993 (2022).
[34] G. Renaud, J. Bosch, A. Van der Steen, and N. de Jong, J. Acoust. Soc. Am. **132**, EL470 (2012).
[35] S. van der Meer, B. Dollet, M. Voormolen, C. T. Chin, A. Bouakaz, N. de Jong, M. Versluis, and D. Lohse, J. Acoust. Soc. Am. **121**, 648 (2007).

[36]A. Prosperetti, J. Acoust. Soc. Am. **61**, 17 (1977).

[37]T. G. Leighton, *The Acoustic Bubble* (Academic Press, 1994).

[38]T. Segers, N. de Jong, and M. Versluis, J. Acoust. Soc. Am. **140**, 2506 (2016).

[39]As demonstrated later, variations in $\sigma(R_0)$ are found, including values close to zero. These result in nonlinear bubble oscillations already at the lowest employed PNP of 7 kPa. When the bubble buckles during its oscillations, χ vanishes and it experiences less resistance against compression than it experiences against expansion. As such, P_A in Eq. (2) was not fixed.

[40]D. Vollhardt and U. Retter, Langmuir **14**, 7250 (1998).

14 June 2024 09:37:01